Materials Transactions, Vol. 44, No. 4 (2003) pp. 504 to 510
Special Issue on Platform Science and Technology for Advanced Magnesium Alloys, II

High-purity Magnesium Coating on Magnesium Alloys by Vapor Deposition Technique for Improving Corrosion Resistance

Harushige Tsubakino[1], Atsushi Yamamoto[1], Shinji Fukumoto[1], Atsushi Watanabe[1,*1], Kana Sugahara[1,*2] and Hiroyuki Inoue[2]

[1]*Graduate School of Engineering, Himeji Institute of Technology, Himeji 671-2201, Japan*
[2]*Graduate School, Osaka Prefecture University, Sakai 599-8531, Japan*

Microstructures in coated magnesium alloy with high purity magnesium fabricated by applying a vacuum deposition technique were investigated. Moreover, relationships between microstructures in coated and un-coated magnesium alloys and corrosion behaviors were interpreted by *in-situ* laser microscopic observations during salt immersion tests. Magnesium with 3N-grade and AZ31 magnesium alloy were used for an evaporation source and a substrate for deposition. Temperature of the substrates was changed resulting in change in temperature profile in a furnace in order to optimize deposition coating conditions for obtaining homogeneous microstructures and thickness in deposited layer. The coated specimen revealed superior corrosion resistance to those on 3N–Mg, AZ31 and AZ91E alloys, and comparable to that on 6N–Mg in salt immersion tests using 3% NaCl solution at 300 K for 587 ks. *In-situ* observations showed that inhomogeneity in microstructures, such as second phases and grain boundary segregations, deteriorate corrosion resistance in magnesium alloys. Therefore, pure magnesium coated layer without inhomogeneity in metallographic and electrochemical meanings can improve the corrosion resistance on magnesium alloys.

(Received October 23, 2002; Accepted January 20, 2003)

Keywords: *magnesium alloy, corrosion rate, deposition, coating, in-situ observation, corrosion behavior*

1. Introduction

Poor corrosion resistance is one of the main disadvantages in magnesium and its alloys. However, the corrosion resistance in high purity magnesium is not so poor but comparable to those on die cast aluminum alloys or carbon steels.[1)] Heavy metal impurities deterioratively affect corrosion resistance on magnesium.[2)] Therefore, in relatively new magnesium alloys such as AZ91E alloy, heavy metal concentrations are controlled to be low by metallographic techniques in order to improve the corrosion resistance.[1)] Limitation in heavy metal concentrations, however, decreases recycleablity in magnesium alloys,[3)] notwithstanding that high recycleability is one of the main advantages in magnesium alloy.

Thus, the authors have proposed a new technique for improving the corrosion resistance without detriment to recycleability, which is a deposition technique.[4–7)] In this technique, magnesium or magnesium alloys are used for an evaporation source and also for substrates. Since a purification process based on the retort effect is included in the technique, the substrate is coated with deposited high purity magnesium layer. Advantages of the technique are as follows: It is not necessary to remove the deposited layer when the coated materials are recycled. Scraps with magnesium alloys can be used for the evaporation source. The process is not energy consuming one and non-toxic one for environment.

In the present study, microstructures in coated layers prepared by the optimized conditions for deposition, and also in the layer fabricated on a substrate with large sizes are investigated. Moreover, relationships between corrosion resistance and microstructures are discussed based on *in-situ* laser microscopic observation during salt immersion test.

2. Experimental Procedures

Commercial grade pure magnesium and magnesium alloys were used, chemical compositions of which are listed in Table 1. Magnesium with 3N grade was used for an evaporation source, while AZ31 magnesium alloy was used for a substrate for deposition. Details of the deposition technique were reported in the previous paper.[6)] In order to obtain the optimum conditions for deposition, temperatures

Table 1 Chemical compositions of magnesium and magnesium alloys (mass%).

	Al	Zn	Mn	Si	Cu	Ni	Fe
3N–Mg	0.004	0.003	0.004	0.005	<0.001	<0.001	0.002
6N–Mg	0.000001	—	0.000005	0.000016	<0.000005	<0.000001	0.000002
AZ31	2.96	0.828	0.433	0.004	0.004	—	0.002
AZ91E	8.1	0.6	0.25	0.03	0.003	<0.001	0.003

*1Graduate Student, Himeji Institute of Technology. Present address: Yamato Scale Co., Ltd., Akashi, Japan.
*2Graduate Student, Himeji Institute of Technology. Present address: Phoenix Electric Co., Ltd., Himeji, Japan.

of the substrate are changed in the range of 500 to 620 K with constant temperature of about 980 K for the evaporation source, which results in changing temperature profile in the furnace. A new deposition coating furnace with large internal sizes was developed based on the knowledge obtained in the previous study, and coating a large substrate with about $60 \times 100 \times 6\,mm^3$ in sizes was attempted.

Salt immersion tests were carried out to evaluate corrosion resistance on the coated specimen together with un-coated specimens for comparison in 3% NaCl solution at 300 K for 587 ks. Corrosion behavior on the specimens were investigated by *in-situ* observations using a laser microscope (1LM15, Lasertec Co.) during immersion tests in 1% NaCl solution at R. T. Specimens for *in-situ* observations were about $10 \times 10 \times 5\,mm^3$ in sizes. The specimens were mechanically grounded, polished by cloth rubbing and etched with an acetic picral etchant (acetic acid: 200 mL, picric acid: 5 g, H_2O: 200 mL, ethanol: 100 mL). Surfaces of the specimens were covered by an organic resin remaining a surface for observation, and then dipped into the solution. Details of the procedures were described in the previous paper.[8)]

Microstructures of the corroded surface after immersion tests were investigated by a scanning electron microscope (SEM: S-900, Hitachi Ltd.) equipped with an energy dispersive X-ray analyzer (EDX).

3. Results and Discussion

3.1 Deposition coating

Optimization of deposition conditions was carried out using the previous furnace which is schematically illustrated in Fig. 1(a). The optimum temperatures for the evaporation source and the substrate were about 983 and 573 K, respectively. The temperature profile is shown in Fig. 1(b). There was a bump between the substrate and the evacuating end. When a profile without the bump was applied for deposition coating, the side surface opposite to the evaporation source was not coated.

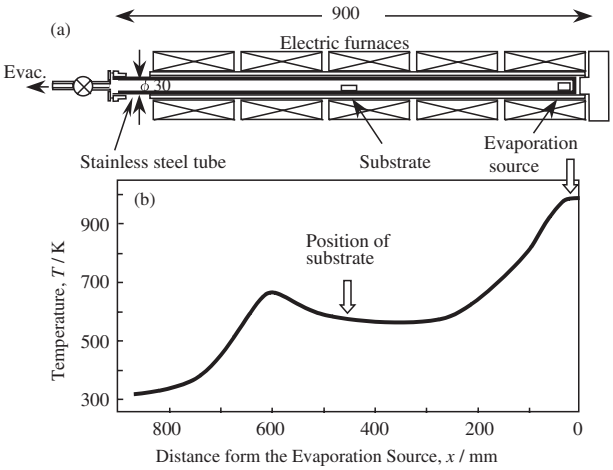

Fig. 1 Schematic illustration of the deposition furnace (a) and temperature profile in the furnace (b).

Cross sections of the coated specimen fabricated with the temperature conditions mentioned above under about 1.5×10^{-3} Pa for 7.2 ks are shown in Fig. 2. Thickness of the deposited magnesium layer on the side surface opposite to the evaporation source was about 6 µm (a) which was comparable to those on the top surface, (b) and (c), and also that on the side surface faced to the evaporation source (d). Homogeneity in thickness has been improved compared with the previous result,[9)] moreover defects such as pores or voids

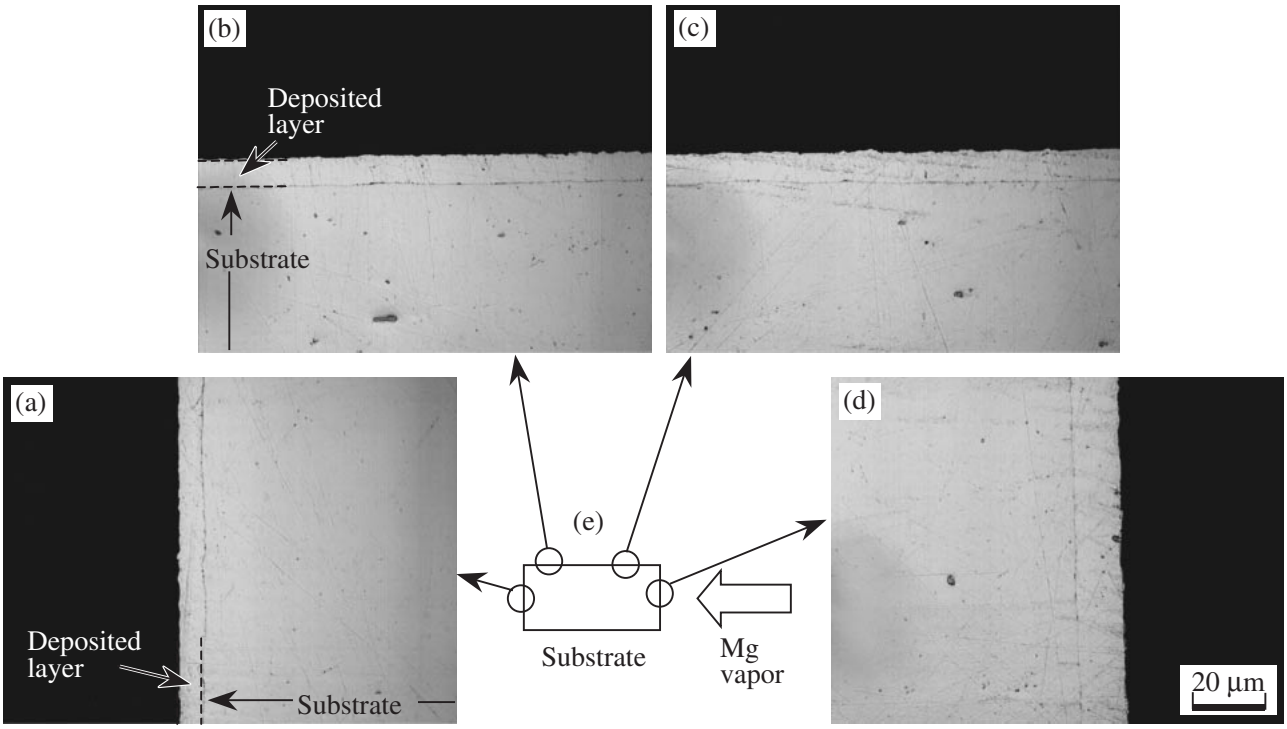

Fig. 2 Cross sections of the coated specimen fabricated at 573 K for 7.2 ks. (a)–(d) show the cross sections taken at each position indicated in (e).

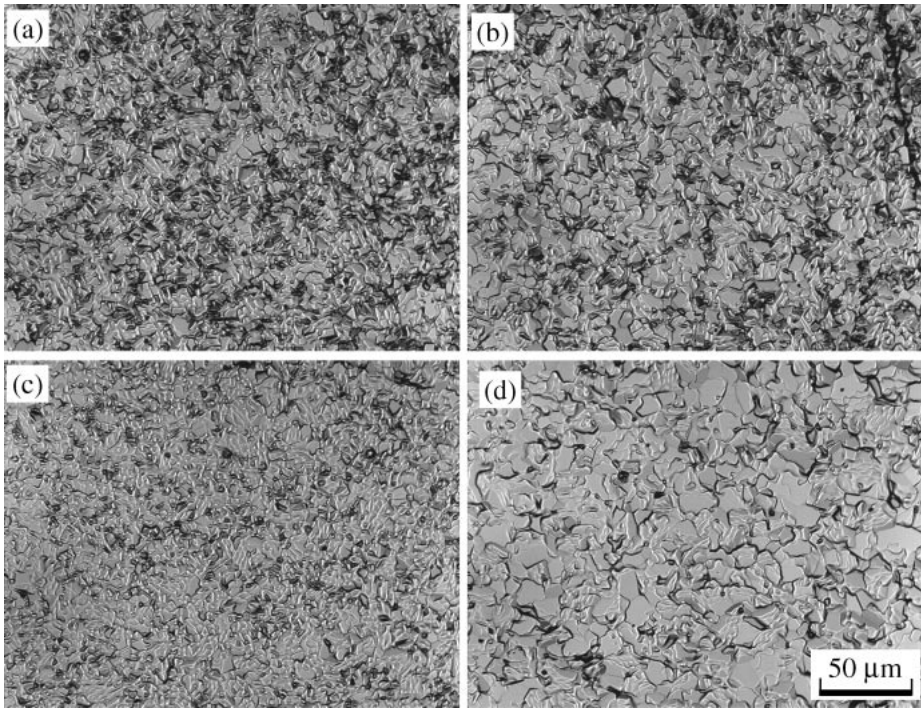

Fig. 3 SEM images of the deposited surfaces (a)–(d) at the positions corresponding with (a)–(d) in Fig. 2, respectively.

at the interface between the substrate and the deposited layer were diminished.

Microstructures of the deposited surfaces corresponding to the cross sections in Figs. 2(a)–(d) are shown in Figs. 3(a)–(d), respectively. Grain sizes varied from about 5 to 20 μm depending on the surfaces, but any defects were not observed. As reported in the previous paper,[6] coating at higher substrate temperature results in deposition of grains with larger sizes. Small grains in the side surface opposite to the evaporation source, (c), imply that the temperature was lower or density of magnesium vapor was lower than those in other surfaces. The latter case seems to be valid referring to the temperature profile in Fig. 1.

The specimen sizes of the substrates used in the above mentioned results were about $10 \times 10 \times 5\,\mathrm{mm}^3$, which seems to be too small for practical applications. Deposition on large specimens with $20 \times 40 \times 6$ and $10 \times 40 \times 6\,\mathrm{mm}^3$ in sizes were attempted under the same conditions as those mentioned above. However, completely coated specimen was not obtained, un-coated portions were remained. It was considered to be due to the small internal sizes of the furnace, about 30 mm in diameter and 900 mm in length. Therefore, a large furnace has been newly developed, in which the internal diameter was about 90 mm and the length was about 1000 mm. Only two furnaces were used for an evaporation source and a substrate. Deposition on a substrate with about $60 \times 100 \times 6\,\mathrm{mm}^3$ in sizes was attempted under about the same temperature profile to that in the small furnace (Fig. 1(b)), however, it resulted in unsuccessful, the specimen could not be coated. Coating of large area of the specimen surfaces occurred at lower substrate temperatures than that for the small furnace, about 400 K. It is considered that the flow of magnesium vapor or density of magnesium vapor was changed by increasing the internal diameter of the furnace. However, the microstructures of the coated layer showed columnar growth of grains, which are shown later. Since the small internal size in the small furnace seems to play a beneficial effect on coating, a condenser with an orifice of about 10 mm in diameter was set between the evaporation source and the substrate.

By using the orifice, deposition occurred at higher temperatures compared with the cases without the orifice. Cross section of the coated specimen prepared at 523 K for 7.2 ks without an orifice is shown in Fig. 4(a), the columnar

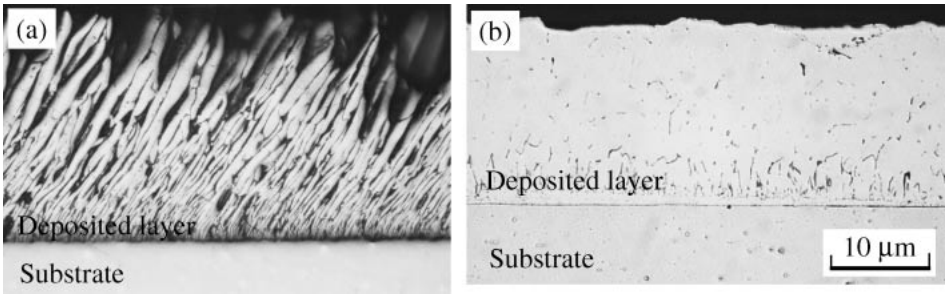

Fig. 4 Microstructures of the deposited layer fabricated using the large furnace at 523 K for 7.2 ks without an orifice (a) and at 573 K for 7.2 ks with an orifice (b).

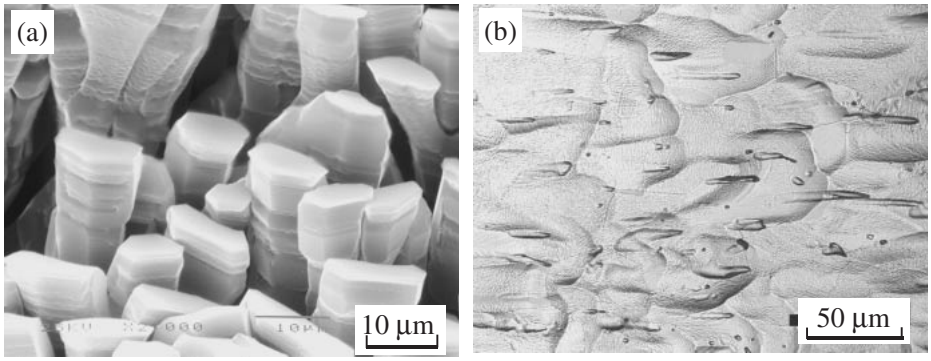

Fig. 5 Surface microstructures of the same specimens in Figs. 4(a) and (b), that is, fabricated at 523 K for 7.2 ks without an orifice (a) and at 573 K for 7.2 ks with an orifice (b).

growth of the grains can be seen. On the other hand, cross section of the coated specimen prepared using an orifice at the substrate temperature of 573 K for 7.2 ks, same as that in the condition for the small furnace, the columnar growth changed into planar growth as shown in Fig. 4(b). Microstructures of the surfaces on the same specimens as Figs. 4(a) and (b) are shown in Figs. 5(a) and (b), respectively. It is considered that there is a predominant crystal orientation for columnar growth which appears at lower substrate temperatures. From a view point of improvement of corrosion resistance, spaces between grains are not favorable.

3.2 Corrosion behaviors

Corrosion rate on the coated specimen of the AZ31 alloy fabricated at 573 K for 7.2 ks together with those on the un-coated 3N–Mg and 6N–Mg, and AZ31 and AZ91E alloys are shown in Fig. 6, the values in which were calculated from weight losses in salt immersion tests at 300 K for 587 ks using a 3% NaCl solution. The corrosion resistance on the coated specimen is superior to those on the un-coated 3N–Mg, AZ31 and AZ91E alloys, and comparable to that on the un-coated 6N–Mg.

In-situ observations of corrosion on the specimens can interpret the reason why the corrosion rates on the un-coated 6N–Mg and the coated specimen are superior to those on others. Figures 7(a) and (b) show the microstructures in the un-coated 3N–Mg before and during a salt immersion test using a 1% NaCl solution at R. T., respectively. There can be seen many inclusions in the specimen which are indicated by the arrows A, B and C in (a). When the specimen was

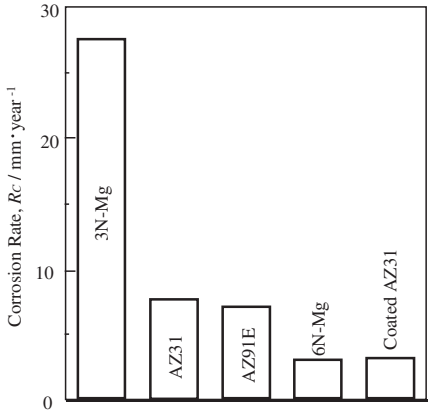

Fig. 6 Corrosion rates calculated from weight losses in a salt immersion tests with 3% NaCl solution at 300 K for 587 ks. The specimens of 3N–Mg, AZ31 alloy, AZ91E alloy and 6N–Mg were un-coated, while the coated specimen was fabricated at 573 K for 7.2 ks in the small furnace.

immersed into the solution, bubbles were observed to be formed at the position A, B and C in (b), that is, the intermetallic inclusions act as the origins of evolution of bubbles. These bubbles are believed to be hydrogen bubbles[10,11] evolved by the following corrosion reaction of magnesium:[12]

$$Mg \rightarrow Mg^{2+} + 2e^{-} \quad (1)$$

$$2H_2O + 2e^{-} \rightarrow H_2 + 2(OH^{-}) \quad (2)$$

$$Mg^{2+} + 2(OH^{-}) \rightarrow Mg(OH)_2 \quad (3)$$

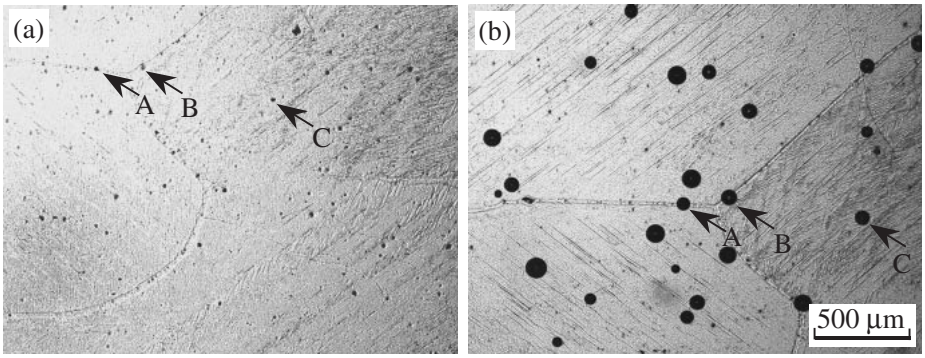

Fig. 7 Microstructure on the specimen of the un-coated 3N–Mg before immersion test (a), and *in-situ* observation of the same specimen during immersion test (b). The arrows A-C in (a) and (b) indicate the same positions, respectively.

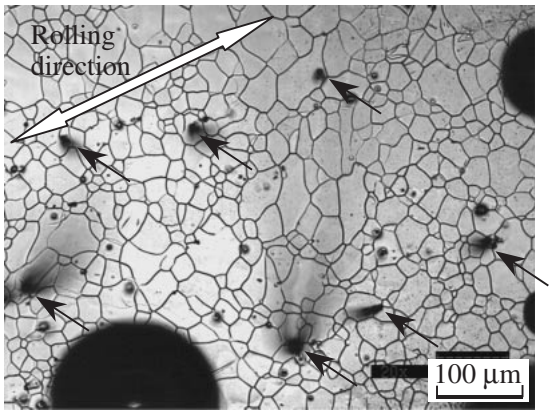

Fig. 8 *In-situ* observation of corrosion reaction on the un-coated AZ31 alloy during a salt immersion test. Dark mist-like contrasts indicated by the black arrows are due to flows of many fine bubbles. Rolling direction in manufacturing process would be parallel to the white arrow.

In the case of the un-coated AZ31 alloy, bubble evolutions were observed as shown in Fig. 8, in which mist-like contrasts indicated by the arrows were due to flows of many small bubbles. Although it is difficult to distingush between bubbles and inclusions, alignment of positions for bubble evolution (indicated by the arrows) along the rolling direction (indicated by the white arrow) implies that inclusions provide the origins for bubble formation.

On the bubble evolution in the un-coated AZ91E alloy, it was observed to be formed at the second phase on a grain boundary as shown in Fig. 9. Song *et al.*[10] reported that the bubbles were formed at the edge of β ($Mg_{17}Al_{12}$) phase, which agree with the present result.

As reported in the previous papers,[8,13] filiform corrosion occurs on the un-coated 3N–Mg and the un-coated AZ31 alloy. *In-situ* observation of filiform corrosion on the un-coated AZ31 alloy is shown in Fig. 10(a). The filiform corrosion occurred at the position indicated by the arrow and then advanced remaining tails. Corrosion reaction occurred at the heads of filiforms, while the tails were inactive. After the *in-situ* observation, the specimen was rinsed and dried, then observed by SEM. The area around the origin is shown in low and high magnifications in (b) and (c), respectively. There can be seen that the filiform corrosion occurred near the inclusion indicated by the arrows. Energy dispersive X-ray analysis showed that the inclusion was a compound with Al–Mn system.

Figures 11(a) and (b) show about the same area on the un-coated AZ31 alloy after 1.86 and 1.92 ks from the start of immersion, respectively. The head advanced about 180 μm for 60 s, from the position indicated by the white arrow toward the positions indicated by the arrows A and B. Detailed observations showed that the filiform corrosion proceeded along grain boundaries. There would be segregation of solute elements on grain boundaries. Inclusions and grain boundaries are inhomogeneous microstructures in metallographic meaning and also in electrochemical meaning, which provide predominant portions for corrosion reactions.

The deposition method intrinsically includes purification process, which results in coating the specimen surfaces with high purity magnesium layer without intermetallic inclusions or segregations. However, evolution of hydrogen bubbles occurred as like as those in the un-coated 3N–Mg and the un-coated AZ31 alloy, although filiform corrosion did not occur on the coated specimens as reported in the previous paper.[8] Figures 12(a) and (b) show the same area in the coated surface in the salt solution. The bubble indicated by the arrow in (b) was formed at the position indicated by the arrow in (a). Careful observations showed that the same position on the dried specimen (c), and then the position was found out by SEM observation (d). High magnification image of the origin on the bubble is shown in (e), fine flakes in which are believed to be magnesium hydroxide formed by corrosion reactions.[14] Bubble evolution occurs at many positions at the beginning of salt immersion test, the other part of the surface is covered with magnesium hydroxide. The positions where bubbles evolve are gradually covered by hydroxide with proceeding immersion, and when the positions are completely covered, bubble formation is diminished as mentioned in the previous paper.[8] Magnesium and oxygen were detected at the position of bubble formation as shown in Fig. 12(e).

Similar corrosion reactions to those on the coated specimen were observed on the un-coated 6N–Mg,[8] that is, only general corrosion occurred without filiform corrosion. Poor corrosion resistance on the un-coated 3N–Mg and the un-coated AZ31 alloy are considered to be due to occurrence of filiform corrosion. On the un-coated AZ91E alloy, filiform corrosion did not occur, but internal regions surrounded by grain boundary β phase are observed to be predominantly corroded, which agree with results reported by Song *et al.*[10] and Lunder *et al.*[15]

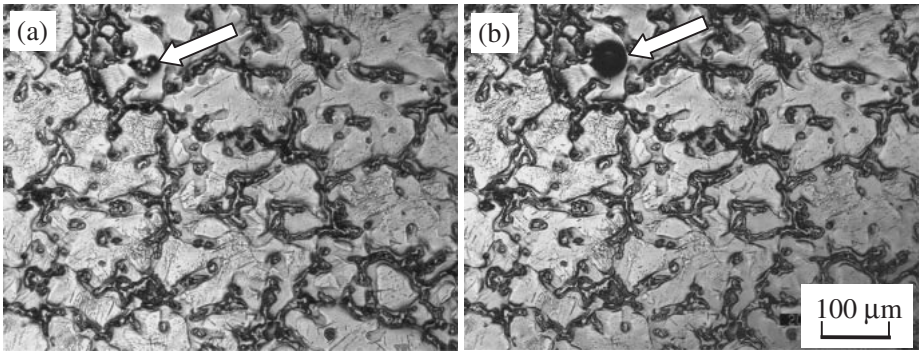

Fig. 9 *In-situ* observation of corrosion reaction in the un-coated AZ91E alloy. Hydrogen bubble indicated by the arrow in (b) were formed at the vicinity of grain boundary indicated by the arrow in (a).

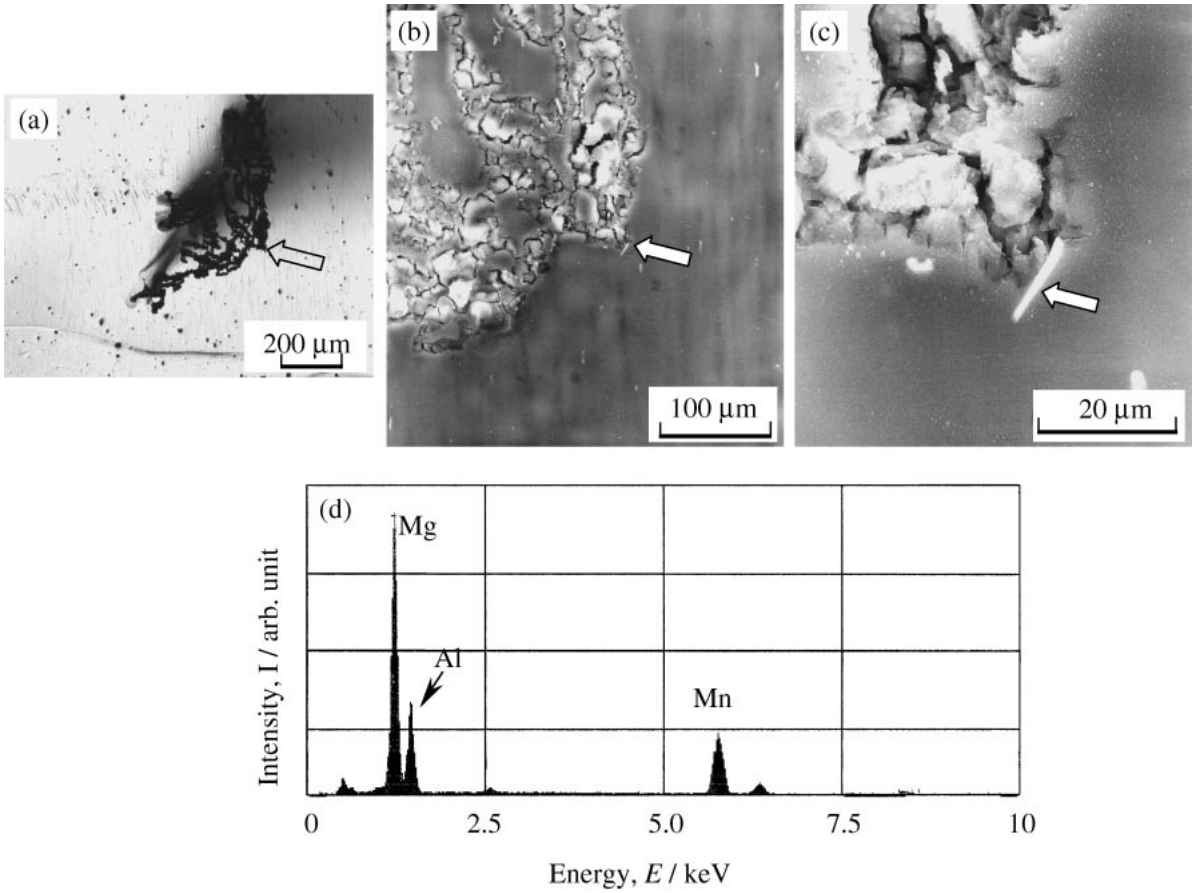

Fig. 10 *In-situ* observation of a filiform corrosion in the un-coated AZ31 alloy (a). SEM image with low and high magnifications (b) and (c), respectively, of the area in (a) after salt immersion test. The arrows in (a), (b) and (c) indicate the origin of the filiform corrosion. EDX spectrum taken at the inclusion indicated in (c).

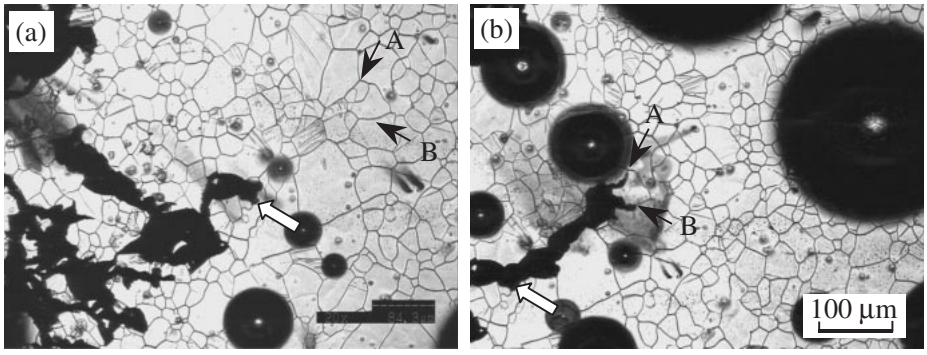

Fig. 11 *In-situ* observation of the filiform corrosion in the un-coated AZ31 alloy. After 1.86 and 1.92 ks from the start of the immersion, (a) and (b), respectively. The filiform corrosion advanced from the position indicated by the white arrow in (a) to A and B through grain boundaries.

Homogeneous microstructures with high purity and without second phases and segregations provide superior corrosion resistance for the coated specimens.

4. Summary

Optimization of deposition conditions has lead to fabrication of coated layers on the substrate with homogeneous thickness and microstructures. A large furnace has been developed, which enables one to perform deposition on a large substrate with $60 \times 100 \times 6\,\mathrm{mm}^3$ in sizes.

The corrosion resistance on the coated specimen is superior to those on the un-coated 3N–Mg, un-coated AZ31 and AZ91E alloys, and comparable to that on the un-coated 6N–Mg.

In-situ observations on salt immersion tests using 1% NaCl solution showed that intermetallic inclusions and grain boundary segregations caused local corrosion such as filiform corrosion on the un-coated 3N–Mg and the un-coated AZ31 alloy, and predominant grain interior corrosion on the un-coated AZ91E alloy. Homogeneous metallography on the coated specimen leads to general corrosion, which results in improving the corrosion resistance in magnesium alloys.

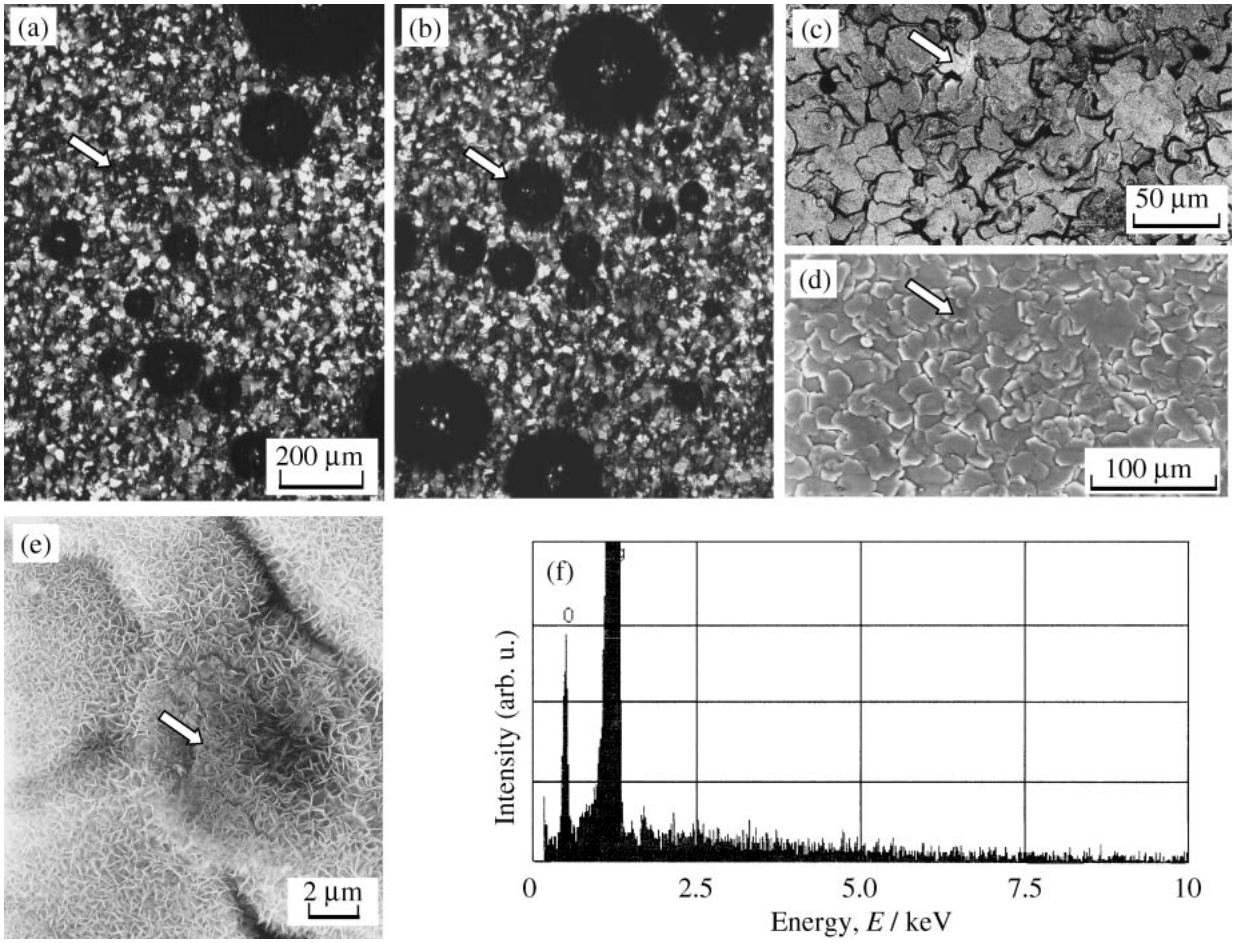

Fig. 12 *In-situ* observations of corrosion reaction in the coated specimen fabricated at 573 K for 7.2 ks in the small furnace; (a) and (b). The bubble indicated by the arrow in (b) was evolved at the position indicated by the arrow in (a). Laser micrograph and SEM image showing the position for bubble evolution, (c) and (d), respectively. High magnification SEM image and EDX spectrum taken at the position for bubble evolution, (e) and (f), respectively.

Acknowledgements

This work was supported by the Priority Group of Platform Science and Technology for Advanced Magnesium Alloys, Ministry of Education, Culture, Sports, Science and Technology, Japan.

REFERENCES

1) K. N. Reichek and J. E. Hillis: SAE Technical Paper Series 850417 (1985) 1–12.
2) J. D. Hanawalt, C. E. Nelson and J. A. Peloubet: Trans. Metall. AIME. **147** (1942) 273–299.
3) H. Wentz and L. Ganim: Light Metal Age **50** (1992) No. 2, 14–21.
4) A. Yamamoto, A. Watanabe, K. Sugahara, T. Tsubakino and S. Fukumoto: Scr. Mater. **44** (2001) 1039–1042.
5) H. Tsubakino, A. Watanabe, A. Yamamoto and S. Fukumoto: Mater. Sci. Forum **350–351** (2000) 235–240.
6) A. Yamamoto, A. Watanbe, K. Sugahara, S. Fukumoto and H. Tsubakino: Mater. Trans. **42** (2001) 1237–1242.
7) H. Tsubakino, A. Yamamoto, A. Watanabe, K. Sugahara and S. Fukumoto: *Proc. 4th Pacific RIM*, (The Japan Inst. Metals, 2001) pp. 1263–1266.
8) A. Yamamoto, A. Watanabe, K. Sugahara, S. Fukumoto and H. Tsubakino: Mater. Trans. **42** (2001) 1243–1248.
9) H. Tsubakino, A. Yamamoto, A. Watanabe and S. Fukumoto: Materials Week 2001 Proc. Inter. Cong. on Advanced Materials and Processings, Munich, Germany, October 2001: CD-ROM, Ed. Werkstoffwoch-Partnerschaft GbR, Germany.
10) G. Song, A. Atrems, D. John and L. Zehn: *Magnesium Alloys and their Applications*, (Wiley-VCH, Weinheim, 2000) 425–431.
11) J. D. Cotton: J. Electrochem. Soc. **136** (1989) 523C–527C.
12) G. L. Maker and J. Kruger: Inter. Mater. Rev. **38** (1993) 138–153.
13) A. Yamamoto, A. Watanabe, K. Sugahara, S. Fukumoto and H. Tsubakino: *Proc. 2nd Inter. Conf. on Environment Sensitive Cracking and Corrosion Damage, ESCCD 2001*, ed. by M. Matsumura *et al.*, (Nichiki Printing, Hiroshima, 2001) pp. 160–167.
14) C. B. Baligaand and P. Tsakiropoulos: Mater. Sci. Technol. **9** (1993) 513–519.
15) O. Lunder, T. K. Aune and K. Nisancioglu: Corrosion **43** (1987) 291–295.